Copyright © 2007 Tech Science Press CMES, vol.22, no.3, pp.165-188, 2007

# A Meshless Local Petrov-Galerkin Method for Magnetic Diffusion in Non-magnetic Conductors

**J.N. Johnson**[1] **and J.M. Owen**[2]

**Abstract:** In this paper, we propose a Meshless Local Petrov-Galerkin method for studying the diffusion of a magnetic field within a non-magnetic ($\mu = \mu_0$) conducting medium with non-homogeneous and anisotropic electrical resistivity. We derive a local weak form for the magnetic diffusion equation and discuss the effects of different trial/test functions and nodal spacings on its solution. We then demonstrate that the method produces convergent results for several relevant one-dimensional test problems for which solutions are known. This method has the potential to be combined with other mesh-free methods such as Smoothed Particle Hydrodynamics (SPH) to solve problems in resistive magnetohydrodynamics, which has several applications in astrophysics, plasma physics, and engineering.

**Keyword:** meshless method, local weak form, magnetic field, diffusion, resistivity, conductivity, conductor, moving least squares, anisotropic, Maxwell's equations, magnetohydrodynamics

## 1 Introduction

The study of magnetic fields within electrical conductors has become an area of great interest in recent years. The dynamics of these systems have applications spanning several length scales in nature and in the laboratory, from astrophysical systems to metalurgy [Davidson (2001)]. In particular, the conductivity of the material in which a magnetic field exists greatly affects the behavior of that magnetic field–in a perfect conductor, the field is "frozen" into the medium and remains stationary with respect to it [Jackson (1999)]; in a conductor with finite conductivity (nonzero resistivity), the magnetic field diffuses out of the medium in some finite amount of time. To describe such magnetic diffusion, it is necessary to accurately represent both the material's conductivity and the governing equations for the magnetic field.

Several methods have been used to study magnetic fields in conducting media. Hyman and Shashkov (2001) describe the application of their Mimetic Finite Difference method to problems in electromagnetics and magnetic diffusion with a spatial discretization that preserves the continuum vector identities. Brauer and Mayergoyz (2004) use a Finite Element method to study eddy currents and magnetic diffusion in magnetic materials in axisymmetric configurations. More recently, the Vector Finite Element (VFE) and Element Free Galerkin (EFG) methods have been applied to these problems [Rieben and White (2006), Bottauscio, Chiampi, and Manzin (2006)]. All of these methods are mesh-based except for the EFG method (though this technique does, in fact, rely upon a background mesh for performing numerical integration).

Mesh-free methods have recently become very popular in the solution of various types of boundary value problems [Belytschko, Krogauz, Organ, Fleming, and Krysl (1996)]. These methods can often adapt easily to the geometry of the problem, and they avoid the need to generate a mesh (a task which can be cumbersome for complex geometries). A particular strength of mesh-free methods is that they are well-suited for describing solutions on sets of moving or disordered points. If the magnetic diffusion problem can be solved with a mesh-free method, this method can also be applied to problems in which the conductor moves, dragging the magnetic field along with it. If this

[1] UC Davis/LLNL, Livermore, CA, USA.
[2] LLNL, Livermore, CA, USA.

method is then combined with another mesh-free method that incorporates deformations in the material, it can be applied to problems in magneto-hydrodynamics (MHD), which describe a broad class of problems from galaxy formation to the magnetic confinement [Chen (1984)] and acceleration [Hwang, Horton, Howard, Evans, and Brockington (2006)] of plasmas.

In this paper, we develop a Meshless Local Petrov-Galerkin (MLPG) method [Atluri and Zhu (1998)] for the solution of the magnetic diffusion equation. This method has been used to model a number of different types of systems, most prominently in solid mechanics problems but also in studying convection-diffusion [Lin and Atluri (2000)], incompressible Navier-Stokes flows [Lin and Atluri (2001)], the heat equation [Sterk, Robic, and Trobec (2005)] and even nanoscale physics [Atluri (2004)]. We choose the MLPG formulation because it has a great deal of flexibility in the representation of the solution and does not rely upon a background mesh for the computation of numerical quadrature. This makes it a truly mesh-free method, suitable for problems in which computational points move and the material becomes increasingly distorted with respect to its initial configuration. We intend eventually to study the equations of resistive MHD by combining this flexible method with a form of Smoothed Particle Hydrodynamics (SPH) [Monaghan (1992), Price and Monaghan (2004)], treating magnetic diffusion with the weak form of the former and the fluid/field $\nabla \times \mathbf{v} \times \mathbf{B}$ and $\mathbf{J} \times \mathbf{B}$ coupling with the strong form of the latter.

In the next section, we derive the magnetic diffusion equation. We develop a local weak form from which we can construct our method in section 3. In section 4 we describe the fully discrete form of the magnetic diffusion equation with time stepping. In section 5 we discuss specific issues with the implementation that affect the accuracy of the solution. We demonstrate the convergence of the method for various one-dimensional test problems using selected variants of the MLPG method in section 6. Section 7 contains the conclusions of the study and outlines future and ongoing work.

## 2 Magnetic Diffusion

The dynamics of electromagnetic fields are described most generally by Maxwell's equations. Those pertaining to the evolution of the magnetic field are:

$$\nabla \times \mathbf{E} = -\frac{\partial \mathbf{B}}{\partial t} \tag{1}$$

$$\nabla \times \mathbf{B} = \mu_0 \mathbf{J} + \mu_0 \varepsilon \frac{\partial \mathbf{E}}{\partial t} \tag{2}$$

$$\nabla \cdot \mathbf{B} = 0 \tag{3}$$

where $\mathbf{B}$ is the magnetic induction in Tesla (T), $\mathbf{E}$ is the electric field in Volts per meter (V/m), $\mathbf{J}$ is the electric current density in Amperes per square meter (A/m$^2$), $\varepsilon$ is the permittivity of the material, and $\mu_0$ is the permiability of free space.

The characteristic time scale for magnetic diffusion is much larger than that for that of the propagation of electromagnetic waves, so we are not interested in the time evolution of $\mathbf{E}$. Rather, we assume that the electrons within a conductor respond instantaneously to the magnetic field. We express this by ignoring the second term in Eq. 2 and using Ohm's Law to relate $\mathbf{E}$ to $\mathbf{J}$ [Chen (1984)]:

$$\mathbf{E} = \boldsymbol{\eta} \cdot \mathbf{J} \tag{4}$$

Here, $\boldsymbol{\eta}$ is the electric resistivity, or inverse conductivity, of the material, expressed in Ohm-meters ($\Omega$-m).

### 2.1 Electrical Resistivity Models

The resistivity $\boldsymbol{\eta}$ can have a scalar or a symmetric tensor value and depends upon the material properties and thermodynamic state of the medium. The resistivity must be positive definite, as the energy deposited by the magnetic field into the material from Joule heating is $\mathbf{J} \cdot \boldsymbol{\eta} \cdot \mathbf{J}$, a quantity that is always positive for non-zero resistivity.

One example of a resistivity model used to treat simple metals is the Bloc-Grüneisen equation [Gruneisen (1933)]:

$$\eta = \eta_0 + A \left( \frac{T}{\Theta} \right)^5 \int_0^{\Theta/T} \frac{x^5}{(e^x - 1)(1 - e^{-x})} dx$$

where $T$ is the metal's temperature, $\Theta$ is its Debye temperature, $\eta_0$ is a "residual resistivity" present because of defect scattering, and $A$ is a constant depending upon the configuration of its electrons. On the other hand, the anisotropic resistivity of a plasma is typically computed using the Spitzer model [Chen (1984)]:

$$\eta_{\|} = 5.2 \times 10^{-5} \frac{Z \ln \Lambda}{T^{3/2}}$$
$$\eta_{\perp} \approx 2\eta_{\|}$$

where $\eta_{\|}$ and $\eta_{\perp}$ denote the diagonal components of the resistivity tensor that are "parallel" and "perpendicular" to the magnetic field in the region, Z is the ion charge number within the plasma, $\Lambda$ is the maximum impact parameter for electron-ion scattering, and $T$ is the temperature of the plasma in electron Volts (eV).

Obviously these two physical models for resistivity differ greatly from one another, and both are very sensitive to the temperature of the material. This underscores the importance in developing a numerical method that can handle inhomogeneous, anisotropic, and strongly dynamic models for electrical resistivity. Presently, though, we will verify the MLPG method for simpler resistivity models while verifying that these basic requirements are met.

### 2.2 The Diffusion Equation

We take Eq. 1 as the basis for evolving the magnetic field. When we combine this equation with Eq. 4 and the truncated form of Eq. 2, we obtain

$$\frac{\partial \mathbf{B}}{\partial t} = -\frac{1}{\mu_0} \nabla \times (\boldsymbol{\eta} \cdot \nabla \times \mathbf{B}) \tag{5}$$

This is our governing equation, with Eq. 3 as a constraint. From the vector identity $\nabla \times \nabla \times \mathbf{A} = \nabla(\nabla \cdot \mathbf{A}) - \nabla^2 \mathbf{A}$, we see that Eq. 5 is a kind of diffusion equation. If we define the magnetic "diffusivity" as

$$D_m = \frac{\max(\eta_{ii})}{\mu_0} \tag{6}$$

then the characteristic time (in seconds) over which a magnetic field decays within a conductor with no external field can be estimated using the usual time scale for diffusion equations:

$$\tau \approx \frac{L^2}{D_m} \tag{7}$$

where $L$ is the characteristic scale length (in meters) of the conductor. Tab. 1 contains some resistivities and values of $D_m$ and $\tau$ for some typical materials of length $L = 1$ m. Clearly, good conductors retain magnetic fields for much longer than poor ones.

Table 1: Resistivities of typical materials[a]

| Material | $\eta$ ($\Omega$-m) | $D_m$ (m$^2$/s) | $\tau$ (s) |
|---|---|---|---|
| Copper | $1.7 \times 10^{-8}$ | 0.014 | 74 |
| Gold | $2.44 \times 10^{-8}$ | 0.0194 | 52 |
| Plasma[b] | $5 \times 10^{-7}$ | 0.4 | 3 |
| Carbon | $3.5 \times 10^{-5}$ | 28 | 0.036 |
| Seawater | 0.20 | $1.6 \times 10^{5}$ | $6.3 \times 10^{-6}$ |
| Glass | $10^{12}$ | $8 \times 10^{17}$ | $10^{-18}$ |

[a] en.wikipedia.org/Resistivity and [Chen (1984)].

[b] Here, we take a "typical" plasma to have thermal energy $K_b T \approx 100$ eV

Note that Eq. 5 can be modified to accomodate materials for which the magnetic permittivity $\mu \neq \mu_0$. In this paper, we restrict our attention strictly to nonmagnetic materials (for which $\mu = \mu_0$).

### 2.3 Boundary conditions

Consider a domain $\Omega$ that is filled with a conducting medium. Let $\Gamma$ represent the boundary of the domain.

If the conductor is surrounded by an external magnetic field $\mathbf{B}_\Gamma(\mathbf{x},t)$, then the value of the magnetic field at the boundary $\Gamma$ of the conductor is given by the following *essential* boundary condition:

$$\mathbf{B} = \mathbf{B}_\Gamma(\mathbf{x},t) \qquad \text{on } \Gamma \tag{8}$$

On the other hand, if a good conductor is connected to a source of electrical current so that a sheet of current $\mathbf{K}(\mathbf{x},t)$ runs across its surface, the tangential components of the magnetic field are

given by the following essential boundary condition [Jackson (1999)]:

$$\begin{aligned} \mathbf{n}\cdot\mathbf{B} &= B_n && \text{on } \Gamma \\ \mathbf{n}\times\mathbf{B} &= \mathbf{K}(\mathbf{x},t) && \text{on } \Gamma \end{aligned} \tag{9}$$

where $\mathbf{n}$ is the outward normal of the boundary, and $B_n$ is the component of $\mathbf{B}$ that is normal to the boundary (also specified). Such surface currents can be used to drive magnetic fields within conductors and form the basis for the acceleration of plasmas [Hwang, Horton, Howard, Evans, and Brockington (2006)]. Thus, we see that our technique must accommodate essential boundary conditions in order to realistically describe problems of interest.

If the electric field $\mathbf{E} = \mathbf{E}_\Gamma$ at the surface of the conductor (for example, if no current enters or exits the conductor through its surface, so that it is electrically insulated), the associated *natural* boundary condition is

$$\mathbf{n}\times\boldsymbol{\eta}\cdot\mu_0\nabla\times\mathbf{B} = \mathbf{n}\times\mathbf{E}_\Gamma \quad \text{on } \Gamma \tag{10}$$

For magnetic materials (those for which $\mu \gg \mu_0$), a discontinuity in the normal component of $\mathbf{B}$ can exist at the material boundary [Jackson (1999)]. We will not discuss these materials here.

### *2.4 The Divergence of* B

An important feature of magnetic fields is that their divergence is exactly zero. A non-zero divergence implies the presence of magnetic "charge" analogous to the electric charge to which the divergence of the electric field is proportional in Poisson's equation of electrostatics:

$$\nabla\cdot\mathbf{E} = \frac{\rho_e}{\varepsilon} \tag{11}$$

The test problems in this study have one-dimensional symmetry so that the $y$ and $z$ derivatives of the magnetic induction are zero, reducing Eq. 3 to

$$\frac{\partial B_x}{\partial x} = 0$$

meaning that $B_x$ cannot depend upon any spatial coordinate. In future work, we will measure any non-zero magnetic divergence and determine whether it dynamically affects the system. Analysis of this sort is especially important in the context of magnetohydrodynamics, where spurious magnetic signals can visit disaster upon the hydrodynamics.

## 3 The Local Weak Form

Consider again a conducting medium within a domain $\Omega$. The medium has a dynamic symmetric-tensor-valued electrical resistivity $\boldsymbol{\eta}(\mathbf{x},t)$ that is related to temperature, density, and other properties. Within the medium is a magnetic field $\mathbf{B}$ given at time $t = 0$ by $\mathbf{B}_0(\mathbf{x},t)$. The initial boundary value problem (IBVP) for the magnetic field is given everywhere in $\Omega$ by Eq. 5 as discussed previously. On the boundary $\Gamma = \Gamma_B \cup \Gamma_K \cup \Gamma_E$, the following boundary conditions hold:

$$\begin{aligned} \mathbf{B} &= \mathbf{B}_\Gamma(\mathbf{x},t) && \text{on } \Gamma_B \\ \mathbf{n}\times\mathbf{B} &= \mathbf{K}(\mathbf{x},t) && \text{on } \Gamma_K \\ \frac{1}{\mu_0}\mathbf{n}\times\boldsymbol{\eta}\nabla\times\mathbf{B} &= \mathbf{n}\times\mathbf{E}_\Gamma && \text{on } \Gamma_E \end{aligned}$$

To devise a MLPG method for this IBVP, we introduce a set of computational points, or *nodes* within $\Omega$ at positions $\mathbf{x}_i$. A weak form for Eq. 5 can then be constructed over a set of local subdomains $\Omega_i$ corresponding to these points. The subdomain $\Omega_i$ represents the support of the $i$th node, and so the subdomains will typically overlap one another and cover the entire global domain $\Omega$. In general, the subdomains may be of any shape or size; presently, we discuss circular subdomains for which the radius of the support of the $i$th point is given by $R_i$.

We write the desired *local* weak form by multiplying both sides of Eq. 5 by a test function $\psi_i(\mathbf{x})$ and integrating over $\Omega_i$:

$$\int_{\Omega_i}\frac{\partial\mathbf{B}}{\partial t}\psi_i d\Omega = -\frac{1}{\mu_0}\int_{\Omega_i}\nabla\times(\boldsymbol{\eta}\cdot\nabla\times\mathbf{B})\,\psi_i d\Omega$$

$\psi$ can be any weight function or mesh-free shape function that has compact support on the subdomain $\Omega_i$. The right hand side of the equation can

be integrated by parts using Green's Theorem for vectors to obtain

$$\int_{\Omega_i} \frac{\partial \mathbf{B}}{\partial t}\psi_i d\Omega = -\frac{1}{\mu_0}\int_{\Gamma_i} \mathbf{n}\times\boldsymbol{\eta}\cdot\nabla\times\mathbf{B}\psi_i d\Gamma + \frac{1}{\mu_0}\int_{\Omega_i}\boldsymbol{\eta}\cdot\nabla\times\mathbf{B}\cdot\nabla\times\psi_i d\Omega \quad (12)$$

Here, $\Gamma_i$ is the intersection of the boundary $\Gamma$ with the subdomain $\Omega_i$ for the $i$th node. In addition, we have defined a curl of the test function $\psi_i(\mathbf{x})$, which we have previously introduced as a scalar function. We will discuss its evaluation shortly.

The first term in the right hand side of Eq. 12 represents the contribution of a natural boundary condition on $\mathbf{B}$. If $\Gamma_i$ intersects $\Gamma_E$, this term may be written as

$$-\int_{\Gamma_i}\mathbf{n}\times\mathbf{E}_\Gamma\psi_i d\Gamma$$

Otherwise, we leave the term in its original form and proceed with our analysis.

### 3.1 Semi-discrete equations

We wish to represent the vector-valued solution for the magnetic field on our set of nodes in $\Omega$. The solution is approximated using a trial function $\phi(\mathbf{x})$ in the usual manner:

$$\mathbf{B}(\mathbf{x},t)\approx\sum_{j\in\Omega_i}\phi_j(\mathbf{x})\hat{\mathbf{B}}_j \quad (13)$$

where $\{\hat{\mathbf{B}}_j\}$ is a set of "fictitious" nodal values representing the projection of $\mathbf{B}(\mathbf{x},t)$ onto the basis $\{\phi_j\}$. $\phi$ can be any mesh-free shape function and is generally different from $\psi$ (since this is a Petrov-Galerkin method). Substituting Eq. 13 into Eq. 12 and pulling the sums outside the integrals yields

$$\sum_j\int_{\Omega_i}\psi_i\phi_j\frac{\partial\hat{\mathbf{B}}_j}{\partial t}d\Omega = -\frac{1}{\mu_0}\sum_j\int_{\Gamma_i}\mathbf{n}\times(\boldsymbol{\eta}\cdot\nabla\times\phi_j)\psi_i\hat{\mathbf{B}}_j d\Gamma + \frac{1}{\mu_0}\sum_j\int_{\Omega_i}\boldsymbol{\eta}\cdot\nabla\times\phi_j\cdot\hat{\mathbf{B}}_j\cdot\nabla\times\psi_i d\Omega \quad (14)$$

Using the fact that $\boldsymbol{\eta}$ is either a scalar or a symmetric tensor, we observe that $\boldsymbol{\eta}\cdot\nabla\times\phi_j\cdot\hat{\mathbf{B}}_j = \hat{\mathbf{B}}_j\cdot\nabla\times\phi_j\cdot\boldsymbol{\eta}$ and so the last term in Eq. 14 becomes

$$\frac{1}{\mu_0}\sum_j\int_{\Omega_i}\hat{\mathbf{B}}_j\cdot(\nabla\times\phi_j\cdot\boldsymbol{\eta}\cdot\nabla\times\psi_i)d\Omega$$

or

$$\frac{1}{\mu_0}\sum_j\int_{\Omega_i}(\nabla\times\psi_i\cdot\boldsymbol{\eta}\cdot\nabla\times\phi_j)\cdot\hat{\mathbf{B}}_j d\Omega$$

Eq. 14 is the MLPG semi-discrete form of the magnetic diffusion equation on the subdomain $\Omega_i$. It is a vector valued equation with 3 components: one for each of the components of the magnetic induction $\mathbf{B}$. At this point, we can follow the common practice for Galerkin and Petrov-Galerkin methods and express this vector equation as a linear system, interpreting $\{\hat{\mathbf{B}}_j\}$ as the components of a solution vector $\mathbf{b}$:

$$\mathbf{M}\frac{\partial\mathbf{b}}{\partial t} = \frac{1}{\mu_0}\mathbf{K}(\boldsymbol{\eta})\mathbf{b} + \frac{1}{\mu_0}\mathbf{f} \quad (15)$$

where $\mathbf{M}$, the "mass matrix," $\mathbf{K}$, the "stiffness matrix," and $\mathbf{f}$, the "boundary vector" are defined as follows:

$$\begin{aligned}\mathbf{M}_{ij} &\equiv \int_{\Omega_i}\psi_i\phi_j d\Omega\\ \mathbf{K}(\boldsymbol{\eta})_{ij} &\equiv \int_{\Omega_i}\nabla\times\psi_i\cdot\boldsymbol{\eta}\cdot\nabla\times\phi_j d\Omega - \int_{\Gamma_i\cup(\Gamma_B\cup\Gamma_K)}\psi_i(\mathbf{n}\times\nabla\times\phi_j)d\Gamma\\ \mathbf{f} &\equiv -\int_{\Gamma_i\cup\Gamma_E}\mathbf{n}\times\mathbf{E}_\Gamma\psi_i d\Gamma\end{aligned} \quad (16)$$

The matrices $\mathbf{M}$ and $\mathbf{K}$ are $3\times3$ matrices, and $\mathbf{b}$ and $\mathbf{f}$ are 3-vectors. If the domain $\Omega$ contains $N$ nodes, the global linear system will thus comprise $N$ linear systems described by Eq. 15 and the solution vector $\mathbf{b}$ will have $3N$ values as expected.

As expected for a MLPG method, $\mathbf{M}$ and $\mathbf{K}$ are not symmetric matrices [Atluri and Zhu (1998), Atluri, Kim, and Cho (1999)]. Consequently, we

do not expect that the fully discrete global linear system will have a symmetric matrix. However, since several freely available linear solvers (for example, PETSc [Balay, Buschelman, Gropp, Kaushik, Knepley, McInnes, Smith, and Zhang (2001)]) can quickly and accurately solve non-symmetric systems, this is not an issue.

### 3.2 Specific forms of matrices

We now obtain explicit expressions for Eq. 16 in terms of the test and trial functions and their partial derivatives. Consider a trial function $\phi_i(\mathbf{x})$. Since electric and magnetic fields are always three-dimensional (even in problems with one-dimensional symmetry), we can treat the function as a scalar function multiplied by the $3\times 3$ identity tensor. Then, if we approximate a vector field $\mathbf{F}$ by

$$\mathbf{F}(\mathbf{x}) = \sum_j \phi_j \hat{\mathbf{F}}_j \tag{17}$$

and its curl by

$$\nabla\times\mathbf{F}(\mathbf{x}) \equiv \sum_j \nabla\times\phi_j\cdot\hat{\mathbf{F}}_j \tag{18}$$

we can equate the components of the curl of Eq. 17 to the components of Eq. 18:

$$\begin{aligned}
[\nabla\times\mathbf{F}(\mathbf{x})]_x &= \sum_{j\in\Omega_i} \phi_{j,y}\hat{F}_z - \phi_{j,z}\hat{F}_y \\
[\nabla\times\mathbf{F}(\mathbf{x})]_y &= \sum_{j\in\Omega_i} \phi_{j,z}\hat{F}_x - \phi_{j,x}\hat{F}_z \\
[\nabla\times\mathbf{F}(\mathbf{x})]_z &= \sum_{j\in\Omega_i} \phi_{j,x}\hat{F}_y - \phi_{j,y}\hat{F}_x
\end{aligned}$$

and can infer that

$$\nabla\times\phi_j(\mathbf{x}) = \begin{pmatrix} 0 & -\phi_{j,z}(\mathbf{x}) & \phi_{j,y}(\mathbf{x}) \\ \phi_{j,z}(\mathbf{x}) & 0 & -\phi_{j,x}(\mathbf{x}) \\ -\phi_{j,y}(\mathbf{x}) & \phi_{j,x}(\mathbf{x}) & 0 \end{pmatrix} \tag{19}$$

where the subscripts $_{,x}$, $_{,y}$, and $_{,z}$ refer to the $x$, $y$ and $z$ derivatives of the trial functions.

A similar analysis of $\mathbf{n}\times\mathbf{F}$ yields

$$\mathbf{n}\times\cdot = \begin{pmatrix} 0 & -n_z & n_y \\ n_z & 0 & -n_x \\ -n_y & n_x & 0 \end{pmatrix} \tag{20}$$

To obtain an expression for $\mathbf{n}\times\nabla\times\phi_\mathbf{j}$, we may take the matrix product of Eq. 20 with Eq. 19. We can use the same method to derive an expression for the curl of the test function $\psi_i(\mathbf{x})$.

Using these definitions of the curl for both the trial and test functions, we can rewrite the matrices and the load vector in Eq. 16 in terms of the shape functions and their partial derivatives, clarifying the analysis. The explicit $3\times 3$ form of the mass matrix is

$$\mathbf{M}_{ij} = \int_{\Omega_i} \begin{pmatrix} \psi_i\phi_j & 0 & 0 \\ 0 & \psi_i\phi_j & 0 \\ 0 & 0 & \psi_i\phi_j \end{pmatrix} d\Omega$$

The stiffness matrix is

$$\begin{aligned}
&\mathbf{K}(\boldsymbol{\eta})_{ij} = \\
&\int_{\Omega_i} \begin{pmatrix} 0 & -\psi_{i,z} & \psi_{i,y} \\ \psi_{i,z} & 0 & -\psi_{i,x} \\ -\psi_{i,y} & \psi_{i,x} & 0 \end{pmatrix} \cdot \begin{pmatrix} \eta_{xx} & 0 & 0 \\ 0 & \eta_{yy} & 0 \\ 0 & 0 & \eta_{zz} \end{pmatrix} \cdot \\
&\quad \begin{pmatrix} 0 & -\phi_{j,z} & \phi_{j,y} \\ \phi_{j,z} & 0 & -\phi_{j,x} \\ -\phi_{j,y} & \phi_{j,x} & 0 \end{pmatrix} d\Omega \\
&- \int_{\Gamma_i\cup(\Gamma_B\cup\Gamma_K)} \psi_i \begin{pmatrix} 0 & -n_z & n_y \\ n_z & 0 & -n_x \\ -n_y & n_x & 0 \end{pmatrix} \cdot \\
&\qquad \begin{pmatrix} 0 & -\phi_{j,z} & \phi_{j,y} \\ \phi_{j,z} & 0 & -\phi_{j},x \\ -\phi_{j,y} & \phi_{j,x} & 0 \end{pmatrix} d\Gamma
\end{aligned} \tag{21}$$

The load vector is

$$\mathbf{f}_i = -\int_{\Gamma_i\cup(\Gamma_B\cup\Gamma_K)} \begin{pmatrix} n_y E_{\Gamma z} - n_z E_{\Gamma y} \\ n_z E_{\Gamma x} - n_x E_{\Gamma z} \\ n_x E_{\Gamma y} - n_y E_{\Gamma x} \end{pmatrix} d\Gamma$$

### 3.3 Meshless Shape Functions

We have mentioned that the trial function $\phi$ and the test function $\psi$ can take various forms. One of the great strengths of the MLPG method is that it allows one to choose these functions from a larger cast of mesh-free shape functions and weight functions that have compact support. These typically include Shepard functions, Moving Least Squares (MLS) functions, Radial Basis

Functions (RBF), and others. These shape functions are extremely popular not only in MLPG methods [Atluri and Zhu (1998)] but also in several other mesh-free methods (Belytschko, Krogauz, Organ, Fleming, and Krysl (1996), Diltz (1999)). There are several excellent expositions of these shape functions in the above references and also in [Atluri (2004), Atluri, Han, and Rajendran (2004)]; for completeness, we briefly describe the MLS shape functions, which we employ in the present method.

Consider a domain $\Omega$ in space in which a continuous function $F$ is defined at several discrete points $\{\mathbf{x}_i\}$. To approximate the value of $F$ at some point $\mathbf{x}$ within this domain, we define the MLS approximant (itself a continuous function of space) as

$$\tilde{F}(\mathbf{x}) = \mathbf{p}^T(\mathbf{x})\mathbf{a}(\mathbf{x}),\ \mathbf{x} \in \Omega \tag{22}$$

where $\mathbf{p}^T(\mathbf{x})$ is some polynomial basis of order $m$ (i.e. $[p_1(\mathbf{x}), p_2(\mathbf{x}), \ldots, p_m(\mathbf{x})]$) and $\mathbf{a}(\mathbf{x})$ is the corresponding projection of $F$ onto that basis. Some examples of $\mathbf{p}^T(\mathbf{x})$ for various dimensions and orders appear below:

$\mathbf{p}^T(\mathbf{x}) = [1, x]$, 1D, linear ($m = 2$)

$\mathbf{p}^T(\mathbf{x}) = [1, x, x^2]$, 1D, quadratic ($m = 3$)

$\mathbf{p}^T(\mathbf{x}) = [1, x, y]$, 2D, linear ($m = 3$)

$\mathbf{p}^T(\mathbf{x}) = [1, x, y, x^2, xy, y^2]$, 2D, quadratic ($m = 6$)

$\mathbf{p}^T(\mathbf{x}) = [1, x, y, z]$, 3D, linear ($m = 4$)

$\mathbf{p}^T(\mathbf{x}) = [1, x, y, z, x^2, xy, y^2, yz, z^2, xz]$, 3D, quadratic ($m$=10)

To project $F$ onto the desired basis, one assumes a set of fictitious nodal values $\{\hat{F}_i\}$ that exist on all points $\{\mathbf{x}_i\}$ within $\Omega$ and then proceeds to minimize a weighted $L_2$ norm defined by

$$J(\mathbf{x}) = \sum_{i \in \Omega} W_i(\mathbf{x}) \left[\mathbf{p}^T(\mathbf{x}_i)\mathbf{a}(\mathbf{x}) - \hat{F}_i\right]^2 \tag{23}$$

where $W_i(\mathbf{x})$ is some compactly-supported weight function centered about the point $\mathbf{x}_i$ in the domain $\Omega$. In general, $\hat{F}_j \neq \tilde{F}(\mathbf{x}_j)$. Rather, the relationship between the fictitious and the "actual" nodal values can be expressed in terms of the desired shape functions $\{\phi_i(\mathbf{x})\}$ as in Eq. 17.

Supposing that there are $N$ points within $\Omega$ and that the dimension of our polynomial basis is $m$, the problem of minimizing Eq. 23 (and thus projecting $F$ onto the basis $\mathbf{p}^T$) is equivalent to solving a least-squares problem described by the $m \times m$ linear system

$$\mathbf{A}(\mathbf{x})\mathbf{a}(\mathbf{x}) = \mathbf{B}(\mathbf{x})\hat{\mathbf{F}} \tag{24}$$

where the matrices $\mathbf{A}$ and $\mathbf{B}$ are defined by

$$\mathbf{A}(\mathbf{x}) = \sum_{i=1}^{N} W_i(\mathbf{x})\mathbf{p}(\mathbf{x}_i)\mathbf{p}^T(\mathbf{x}_i)$$

$$\mathbf{B}(\mathbf{x}) = [W_1(\mathbf{x})\mathbf{p}(\mathbf{x}_1), \ldots, W_N(\mathbf{x}_N)]$$

and $\hat{\mathbf{F}}$ is the vector of fictitious nodal values $\{\hat{F}_i\}$. Note that $\mathbf{A}$ and $\mathbf{B}$ are $m \times m$ and $m \times N$ matrices, respectively. Thus, $\mathbf{a}(\mathbf{x})$, the projection of $F$ onto $\mathbf{p}^T(\mathbf{x})$, becomes $\mathbf{A}^{-1}(\mathbf{x})\mathbf{B}(\mathbf{x})\hat{\mathbf{F}}$ and we obtain the MLS shape functions $\{\phi_i(\mathbf{x})\}$, defined by

$$\phi_i(\mathbf{x}) = \sum_{j \in \Omega} p_j(\mathbf{x})[\mathbf{A}^{-1}(\mathbf{x})\mathbf{B}(\mathbf{x})]_{ji} \tag{25}$$

The *moment matrix* $\mathbf{A}$ is symmetric, and so as long as it is nonsingular, Eq. 24 can be solved using Cholesky factorization. In practice, one can ensure that $\mathbf{A}$ is positive definite by choosing sufficient numbers of points in the neighborhood of $\mathbf{x}$. A rule of thumb adopted by many practitioners is to choose $m$ as roughly twice the number of points as is needed to find a unique solution. This helps to ease difficulties encountered in regions where $F$ is not smooth.

The partial derivatives of these shape functions can be obtained directly using the expression

$$\frac{\partial \phi_i}{\partial x_k} = \sum_{j=1}^{q} \left[\frac{\partial p_j}{\partial x_k}(\mathbf{A}^{-1}\mathbf{B})_{ji} + p_j(\mathbf{A}^{-1}\frac{\partial \mathbf{B}}{\partial x_k} + \frac{\partial \mathbf{A}^{-1}}{\partial x_k}\mathbf{B})_{ji}\right] \tag{26}$$

(where $\frac{\partial \mathbf{A}^{-1}}{\partial x_k} = -\mathbf{A}^{-1}\frac{\partial \mathbf{A}}{\partial x_k}\mathbf{A}^{-1}$) [Atluri and Zhu (1998)], or by using the "diffuse derivatives" explored by Nayroles, Touzot, and Villon (1992). Presently, we directly compute the derivatives using Eq. 26.

As we have mentioned, each mesh-free shape function is constructed using a weight function with compact support [Atluri and Zhu (1998)]. Our implementation uses a quartic spline function identical to that used in several previous studies of MLPG methods:

$$W_i(\xi) = \begin{cases} 1 - 6\xi^2 + 8\xi^3 - 3\xi^4 & 0 \le \xi < 1, \\ 0 & \xi \ge 1. \end{cases} \tag{27}$$

Here, $\xi \equiv |\mathbf{x} - \mathbf{x}_i|/R_i$, where $R_i$ is the radius of support of $W_i$ about $\mathbf{x}_i$.

Atluri, Kim, and Cho (1999) have found that the convergence rates for Shepard functions and MLS functions exceed $h$-convergence, which is given for computed and exact solutions $u_c$ and $u_e$:

$$\|u_c - u_e\| \propto h^{m+1-k} \tag{28}$$

where $\|\cdot\|_k$ is the $k$-norm in the Sobolev space and $m$ is the order of completeness in the polynomial interpolation. We have verified that $h$-convergence is indeed a conservative estimate for the convergence of the interpolation error of the mesh-free shape functions. The MLPG method, like any weak form, is based upon the integration of interpolated quantities, so the convergence rates of the meshless interpolation functions represent a characteristic rate of convergence in the spatial discretization for methods that use them.

In the MLPG framework, $\psi$ can assume a different form than $\phi$. Several popular variants of MLPG exist in the literature (for example, MLPG1-6 [Atluri (2004)]), each one prescribing a relationship between these two functions. Here we focus our attention on the MLPG1 method, which specifies that $\phi$ is one of the aforementioned mesh-free shape functions, and that $\psi$ is the aforementioned weight function $W$ that was used in the construction of $\phi$. This is the original version of the MLPG method and produces accurate results, but suffers from complexities in numerical integration that will be discussed in Section 5. Another variant based upon MLPG5 has been demonstrated by Atluri, Han, and Rajendran (2004) to alleviate these difficulties by eliminating the numerical integration in the stiffness matrix and shows even better accuracy. More recently, a MLPG method based upon a generalized finite difference method has been described by Atluri, Liu, and Han (2006b); this method avoids the the direct differentiation of the shape functions, using the nodal quantities to compute derivatives instead. We hope to explore these variants in the future.

### 3.4 Current density

Once the magnetic diffusion has been solved and the magnetic induction $\mathbf{B}$ obtained, the current density $\mathbf{J}$ can be computed using the truncated form of Eq. 2:

$$\mathbf{J} = \frac{1}{\mu_0} \nabla \times \mathbf{B} \tag{29}$$

Using the definition of the curl given by Eq. 19, we can relate the current density to the fictitious nodal values $\{\hat{\mathbf{B}}\}$:

$$\mathbf{J}(\mathbf{x}) = \sum_{j \in \Omega_i} \begin{pmatrix} 0 & -\phi_{j,z}(\mathbf{x}) & \phi_{j,y}(\mathbf{x}) \\ \phi_{j,z}(\mathbf{x}) & 0 & -\phi_{j,x}(\mathbf{x}) \\ -\phi_{j,y}(\mathbf{x}) & \phi_{j,x}(\mathbf{x}) & 0 \end{pmatrix} \begin{pmatrix} \hat{B}_{xj} \\ \hat{B}_{yj} \\ \hat{B}_{zj} \end{pmatrix} \tag{30}$$

where the subscripts $_{,x}$, $_{,y}$, and $_{,z}$ refer to the $x$, $y$ and $z$ derivatives of the trial functions.

## 4 Time Integration

The characteristic time scale over which diffusion occurs (Eq. 7) can serve as a CFL-like relationship between the time step size and the nodal spacing. Unfortunately, if one adopts this approach, one finds quickly that a time step that scales quadratically with the nodal spacing becomes impractically small for realistic problems. To avoid this issue, we adopt a variable, implicit, Crank-Nicholson-based time integration method that has become popular for solving diffusion and diffusion-like equations [Chinchapatnam, Djidjeli, and Nair (2006), Rieben and White (2006)]. We begin with our semi-discrete linear system (Eq. 15), using a superscript $n$ to denote quantities that are time-centered about the time $t_n$. Here, we

introduce a weighting factor $\theta$ (with $0 \leq \theta \leq 1$) to control the "implicitness" of the time discretization:

$$\mathbf{M}\left(\frac{\partial \mathbf{b}}{\partial t}\right)^{n+\frac{1}{2}} = \frac{1}{\mu_0}\mathbf{K}(\boldsymbol{\eta}^{n+\theta})\mathbf{b}^{n+\theta} \tag{31}$$

We then approximate

$$\left(\frac{\partial \mathbf{b}}{\partial t}\right)^{n+\frac{1}{2}} \approx \frac{\mathbf{b}^{n+1}-\mathbf{b}^{n}}{\Delta t}$$

and

$$\mathbf{b}^{n+\theta} \approx \theta \mathbf{b}^{n+1} + (1-\theta)\mathbf{b}^{n}$$

where $\Delta t = t^{n+1} - t^n$, rearranging the terms to obtain

$$\left[\mathbf{M} - \theta\Delta t\mu_0^{-1}\mathbf{K}(\boldsymbol{\eta}^{n+\theta})\right]\mathbf{b}^{n+1} = \left[\mathbf{M} + (1-\theta)\Delta t\mu_0^{-1}\mathbf{K}(\boldsymbol{\eta}^{n+\theta})\right]\mathbf{b}^{n} + \frac{1}{\mu_0}\mathbf{f}^{n} \tag{32}$$

This linear system must be solved for each time $t_n$ to evolve the magnetic induction to its state at time $t^{n+1}$. The time integration scheme is unconditionally stable for $\theta \geq 1/2$. If $\theta = 0$, we recover the explicit Forward Euler integration method. If $\theta = 1$, this discretization gives us the implicit Backward Euler scheme. Both of these are first-order accurate in time. If $\theta = 1/2$, we get the second-order Crank-Nicholson scheme. With this scheme, we can scale the time step size linearly with the nodal spacing and still obtain accurate, stable results.

Note that $\theta$ also determines the time centering of the electrical resistivity $\boldsymbol{\eta}$ in Eq. 31, which must be computed at $t^{n+\theta} = t^n + \theta\Delta t$. This is crucial if one wishes to obtain the predicted convergence rate for the selected time discretization.

For the test problems in this paper, we use $\theta = 1/2$ and scale the maximum time step size down with the nodal spacing to control the amount of time discretization error in the solution. If one were to use a value of $\theta$ less than 1/2, one must take care to ensure that the spectral radius of the amplification matrix

$$\mathbf{A} = \left[\mathbf{M} - \theta\Delta t\mu_0^{-1}\mathbf{K}(\boldsymbol{\eta}^{\boldsymbol{n}})\right]^{-1} \cdot \left[\mathbf{M} + (1-\theta)\Delta t\mu_0^{-1}\mathbf{K}(\boldsymbol{\eta}^{\boldsymbol{n}})\right]$$

is less than 1 in order to achieve stability [Stoer and Bulirsch (1991)]. Alternatively, one may use Eq. 7 as an estimate for the maximum time step (though this becomes impractical as the nodal spacing in a problem becomes small). In practice, one must be careful even when $\theta = 1/2$, as problems with discontinuities may develop oscillations; these can be eliminated by increasing $\theta$ or more carefully controlling the time step size.

## 5 Implementation

In this section we discuss various issues in the implementation of the technique. The truly meshfree nature of the MLPG method gives it many advantages over other techniques that rely upon some sort of regular connectivity, but the use of overlapping subdomains also complicates the algorithm in areas that are straightforward in other methods.

### *5.1 Numerical Quadrature*

In the computation of the mass and stiffness matrices defined by Eq. 16, the Meshless Local Petrov-Galerkin method produces integrands with complicated shapes. The shape functions are typically ratios of piecewise polynomials, so straightforward Gaussian integration cannot be relied upon to obtain precise results. Atluri, Kim, and Cho (1999) provides an excellent discussion of the trouble encountered by naively using Gauss integration with these techniques, and recommends the use of partitioned integration, with each partition containing a different region of overlapping trial and test functions. We have found that this type of partitioning is more accurate and efficient than performing the integration on a single region with large numbers of Gauss points.

In our numerical experiments, we use a one-dimensional distribution of points like that shown in Fig. 1. Each point $x_i$ has a support domain $\Omega^i_{Tr}$ on which the trial function $\{\phi_i\}$ is defined and in which its neighbor points may be found. Meanwhile, the test function $\psi_i$ is defined on a subdomain $\Omega^i_{Te}$ (which we have previously called simply $\Omega_i$) that is typically smaller than $\Omega^i_{Tr}$. Each of

the integrals in Eq. 16 is evaluated over $\Omega^i_{Te}$.

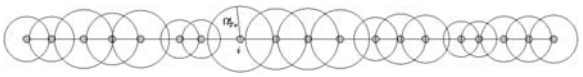

Figure 1: 1D point distribution

To perform this integration, we divide $\Omega_{Te}$ into several partitions, each of which contains a region where $\psi_i$ and $\{\phi_j\}$ overlap in a specific way, as shown by the intervals $I_1$, $I_2$, and $I_3$ in Fig. 2. We perform the integration over each partition with a Gauss quadrature rule. By guaranteeing that the form of the integrand remains the same over each partition, we can obtain accurate results without resorting to integration rules of extremely high order. We have used a 15-point Gauss integration rule and obtained very good results.

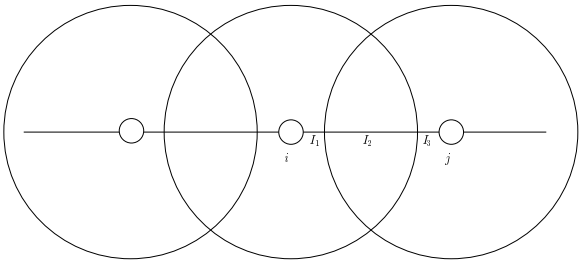


Figure 2: 1D integration segments

### 5.2 Essential Boundary Conditions

Since our method is based on local weak forms, the values of the solution incorporate all points within their subdomains. This makes it difficult to enforce essential boundary conditions directly even when trial functions possessing the Dirac delta function property are used [Atluri, Han, and Rajendran (2004)]. One way to indirectly impose values on the boundary $\Gamma$ of the domain $\Omega$ is to use a penalty method with some multiplier $\alpha \gg 1$. This adds the effect of a strong spring on the boundary that holds the solution at the prescribed value. In this case, penalty terms

$$\alpha \int_{\Gamma_i} \psi_i(\mathbf{x})\phi_j(\mathbf{x})d\Gamma$$

and

$$\alpha \int_{\Gamma_i} \mathbf{B}_\Gamma(\mathbf{x})\psi_i(\mathbf{x})d\Gamma$$

are added to the left and the right hand sides of Eq. 14, respectively. A problem with this approach is that $\alpha$ must be "big enough" so that the penalty terms overshadow the others, but not so large that it renders the matrix ill-conditioned. In other words, $\alpha$ is a free parameter that can be sensitive to the nodal spacing in the problem, meaning that it must vary with the resolution. Nevertheless, it is a straightforward approach that gives convergent solutions. We have found that values of $\alpha$ between $10^6$ and $10^8$ give the best results when using MKS units (in which $\mu_0 = 4\pi \times 10^{-7}\mathrm{N}\cdot\mathrm{A}^2$).

Other approaches have been suggested. The *transformation* method, described in Atluri, Kim, and Cho (1999), imparts the Dirac delta function property to the solution at the boundary via a transformation of the linear system Eq. 32. The transformation matrix $\{R_{ij}\} = \{\phi_j(\mathbf{x}_i)\}^{-1}$ can be computed using LU decomposition to invert the matrix of trial functions, but care must be taken to mitigate numerical errors and the expense of transforming the system. A *modified colocation* method, described in Zhu and Atluri (1998), uses the interpolation

$$\mathbf{B}(\mathbf{x}_i,t) = \sum_{j\in\Omega_i} \phi_j(\mathbf{x}_i)\hat{\mathbf{B}}(t)$$

to replace each row of Eq. 32 corresponding to a node on $\Gamma$, with the right hand side set to the value prescribed by the function $\mathbf{B}_\Gamma$.

$$\sum_{j\in\Omega_i} \phi_j(\mathbf{x}_i)\hat{\mathbf{B}}(t) = \mathbf{B}_\Gamma(\mathbf{x}_i,t), i \in \Gamma \tag{33}$$

Here, one must be careful to eliminate all other entries on these boundary rows in order to avoid introducing spurious errors on the boundary. More recently, Atluri, Liu, and Han (2006a) have described the application of this method to their "mixed" finite-volume MLPG approach in elasticity problems.

We have used both the penalty method and the modified colocation method and have found that

both give convergent results for our test problems. However, the treatment of essential boundary conditions for this method remains an open issue, as surfaces in two and three dimensions are invariably more complicated.

#### 5.2.1 *The* $\mathbf{n}\times\mathbf{B}$ *boundary condition*

When we discuss essential boundary conditions, it is clear that we mean those such as Eq. 8. However, the aforementioned techniques also apply to Eq. 9, which is equivalent to the former in the following sense: if we take the cross product of both sides of $\mathbf{n}$ with Eq. 9 and use the vector identity

$$\mathbf{n}\times(\mathbf{n}\times\mathbf{B}) = \mathbf{n}(\mathbf{n}\cdot\mathbf{B}) - \mathbf{B}(\mathbf{n}\cdot\mathbf{n})$$

we obtain an equation relating $\mathbf{B}$ directly to $B_n$ and $\mathbf{K}$:

$$\mathbf{B} = B_n\mathbf{n} - \mathbf{n}\times\mathbf{K} \quad \text{on } \Gamma \tag{34}$$

This equation is substantially equivalent to Eq. 8, with the functions $B_n(\mathbf{x},t)$ and $\mathbf{K}(\mathbf{x},t)$ specifying the value of $\mathbf{B}$ at the boundary.

### 5.3 *Domains of Support, Condition Number*

We have briefly mentioned the distinct support domains for the trial and test functions ($\Omega^j_{Tr}$ and $\Omega^i_{Te}$, respectively) and that their sizes are typically different. It is crucial to choose proper sizes for these domains, since the accuracy of the solution depends upon both the reproducibility of the mesh-free shape functions and the conditioning of the linear system. We now discuss some rules of thumb for choosing the radii of support for the test and trial functions with these factors in mind.

A trial function at $x_i$ interpolates very accurately in the interior of $\Omega^i_{Tr}$, but not near its boundary. This means that one should evaluate $\phi_i(\mathbf{x})$ only in its interior. Since we only evaluate the trial functions within the subdomain of the test functions, we can accomplish this by making $\Omega^i_{Te}$ smaller than $\Omega^i_{Tr}$. However, the test functions $\{\psi_i\}$ should overlap one another so that Eq. 32 is satisfied everywhere on the global domain $\Omega$. A typical choice for $\Omega^i_{Te}$ is some small multiple of the nodal spacing $h$. We choose the radius of the support for the test functions to be $0.9h$, a setting that has been advocated for the MLPG1 variant by Atluri and Zhu (1998) and Atluri, Kim, and Cho (1999).

On the other hand, we cannot make the trial function support radius too large, since this can smooth out important features in the solution. It can also worsen the condition number $C$ of the matrix in Eq. 32. Tab. 2 shows some condition numbers that result when the radius of $\Omega^i_{Tr}$, $R_{Tr}$, is chosen as a multiple of the nodal spacing $h$. Note that because of the factor of $1/\mu_0 = 7.95\times10^5$ in the stiffness matrix, it is wise to use diagonal scaling before solving the linear system, rendering the system numerically "dimensionless" and reducing the condition number. It is evident $C$ increases with both the resolution of the problem and $R_{Tr}$. Earlier studies of the MLPG1 method used $R_{Tr} = 5h$ in order to make sure that the mesh-free shape functions incorporated enough neighbor values, but more recent studies have shown that lower values will produce more accurate results. In particular, a "mixed" MLPG method for elasticity described by Atluri, Han, and Rajendran (2004) has been developed in order to reduce $R_{Tr}$ while retaining the accuracy of the trial functions. We have found that $R_{Tr}\approx 3h$ works quite well for second order MLS shape functions, and that this radius can be decreased for the shape functions of lower-order consistency.

The condition numbers in Tab. 2 were computed

Table 2: Typical condition numbers

| $h$ | $R_{Tr}/h$ | $C$ (no scaling) | $C$ (scaling) |
|---|---|---|---|
| 0.01 | 3 | $6.3\times10^7$ | 830 |
| 0.005 | 3 | $9.2\times10^8$ | 2200 |
| 0.0025 | 3 | $1.4\times10^{10}$ | 6500 |
| 0.00125 | 3 | $2.2\times10^{11}$ | 21000 |
| 0.01 | 4 | $3.6\times10^8$ | 6000 |
| 0.005 | 4 | $5.5\times10^9$ | 12300 |
| 0.0025 | 4 | $8.6\times10^{10}$ | 25000 |
| 0.00125 | 4 | $1.4\times10^{12}$ | 51000 |
| 0.01 | 5 | $2.5\times10^9$ | 57000 |
| 0.005 | 5 | $1.6\times10^{11}$ | $4.8\times10^5$ |
| 0.0025 | 5 | $1.4\times10^{12}$ | $5.9\times10^5$ |
| 0.00125 | 5 | $2.6\times10^{13}$ | $5.1\times10^6$ |

numerically using $C = \|\boldsymbol{A}^{-1}\|\|\boldsymbol{A}\|$, where $\boldsymbol{A}$ is the matrix on the left-hand side of Eq. 32, and $\|\cdot\|$ is the 2-norm of the matrix.

## 6 Verification

The following test problems have been chosen to verify the present method. We first demonstrate that the method can evolve a Gaussian pulse (the fundamental solution to the diffusion equation) with scalar and tensor resistivities. A square pulse is then evolved to show that the method can achieve the expected convergence rate (first order) for a discontinuous solution. Because we intend later to use this technique to model problems with moving conductors, we evolve moving pulses to show that MLPG can accommodate a moving coordinate frame. We then demonstrate that the technique can reproduce the well-known Fourier series solutions for the diffusion equation with both natural and essential boundary conditions. Then, to test the capability of the method to represent dynamic essential boundary conditions, we impose an oscillating magnetic field on one surface of a medium and evolve the resulting field on the interior. Finally, to test the ability of the method to treat inhomogeneous and time-dependent resistivities, we use the Method of Manufactured Solutions (MMS) to test nonlinear diffusion problems.

Most of the test problems are run with 100, 200, 400, 800, 1600, and 3200 nodes so that accurate estimates for orders of convergence are obtained, and to verify that the conditioning of the linear system does not cripple the technique at higher resolutions. The last three problems, which are based upon the Method of Manufactured Solutions, are run with 25, 50, 100, and 200 nodes, since they exhibit time-dependent resistivity models implemented in an interpreted language, making larger studies less practical. Regardless, we are able to establish evidence of convergence in all cases.

We study both the convergence of the magnetic induction **B** and the current density **J**, related to the former by Eq. 29 and computed using Eq. 30. Convergence rates are measured for the $L_1$, $L_2$, and $L_\infty$ norms of the error in the solution, where these norms are defined as

$$L_p(q) = \left( \frac{\sum_{i=1}^{N} q_i - q_i^e}{N} \right)^{1/N} \qquad (35)$$
$$L_\infty(q) = \max_{1 \le i \le N} |q_i - q_i^e|$$

where $q$ is the quantity under consideration, $q_i$ is its computed solution at the point $\mathbf{x_0}$, and $q_i^e$ is the corresponding exact solution. In the problems presented, we expect second-order convergence in these norms, as dictated by our Crank-Nicholson time discretization. The exception is to this rule is the square pulse decay problem, which has discontinuous initial conditions and therefore should converge at first order.

We use second order MLS shape functions as the trial functions for these test problems, and the test functions are simply the spline functions $W$ (Eq. 27) used to construct the trial functions. The radius of $\Omega_{Tr}$ ($\rho$) is taken to be $3h$, and the radius of $\Omega_{Te}$ is $0.9h$.

To solve the linear system in Eq. 32, we use a Generalized Minimum Residual (GMRES) iterative solver with a residual error tolerance of $10^{-18}$. We use diagonal scaling to remove the factor of $1/\mu_0$ and reduce the condition number of the matrix before solving the system.

It is worth noting that in 1D problems (those that only vary along one spatial dimension, in which $\frac{\partial}{\partial y} = \frac{\partial}{\partial z} = 0$), the $x$ component of the magnetic induction remains constant according to Eq. 3. Therefore, we will only discuss the evolution of $B_y$ and $B_z$ in the test problems.

To test the sensitivity of the technique to irregularities in the point distribution, we run each problem both on a uniform line of points and on a randomly distorted distribution. In this distorted configuration, a point may be displaced to the left or right of its "uniform" position by up to 20% of the nodal spacing $h$. No attempt is made to adjust the support radii of the trial functions to accommodate these distortions–thus, we measure the degree to which variations in neighbors affects the accuracy of the solution.

### 6.1 Gaussian Pulse

Consider a slab of conducting material on $[-L/2, L/2]$ with some resistivity $\boldsymbol{\eta}$ in which a magnetic field exists at time $t = 0$. If there is no magnetic field outside the material, the interior field will decay according to Eq. 5. It is well known that the fundamental solution of diffusion equations with diffusivity $D$ is the Gaussian pulse defined by

$$G_D(x,t) = \frac{1}{\sqrt{4\pi aDt}} \exp\left(\frac{-x^2}{4a}\right) \tag{36}$$

where $a$ is a number (e.g. $1.0 \times 10^{-3}$) characterizing the width of the pulse. The corresponding non-zero component of the current density is

$$J_{G_D}(x,t) = -\frac{1}{2a\mu_0} x G_D(x,t) \tag{37}$$

We will explore solutions of this form for different resistivities and their corresponding magnetic diffusivities given by Eq. 6. Problems of this type allow us to test the effectiveness of the MLPG method in capturing the solution on the interior of $\Gamma$ without regard to boundary conditions, a logical first step in verification.

In these decay problems, we use homogeneous natural boundary conditions, which do not correspond to those of the exact solutions, but are simple to implement. The actual solutions require an approach that represents an infinite or semi-infinite domain either through integral transforms [Lin and Atluri (2000)] or through "infinite element" methods [Zienkiewicz and Taylor (1989)], neither of which we have explored. To get around this discrepancy, we do not evolve the solution all the way out to the boundary.

#### 6.1.1 Scalar Resistivity

Suppose the conducting medium has a scalar resistivity $\eta = \mu_0/100$, and that the only nonzero component of the initial magnetic induction is $B_y$. Then the magnetic diffusivity $D_m$ is 1/100, and we prescribe $B_y(x,0) = G_{1/100}(x,0)$ (with $a = 10^{-3}$) and evolve it until time $t = 0.25$ s. Computed and analytic solutions at this time are shown in Fig. 3.

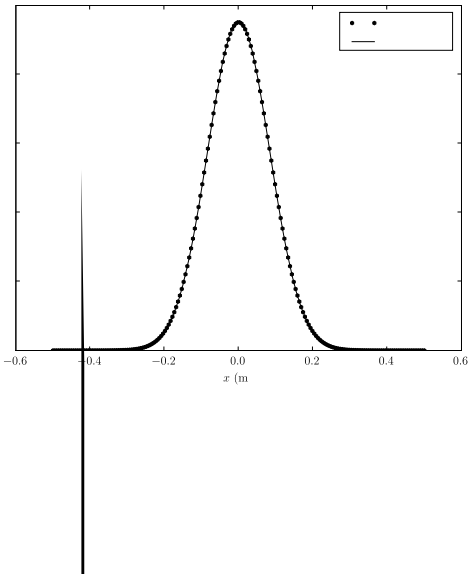

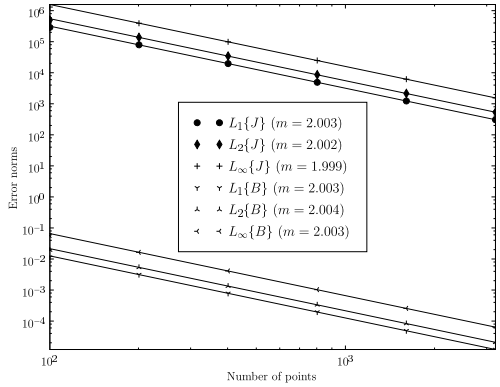


(a)

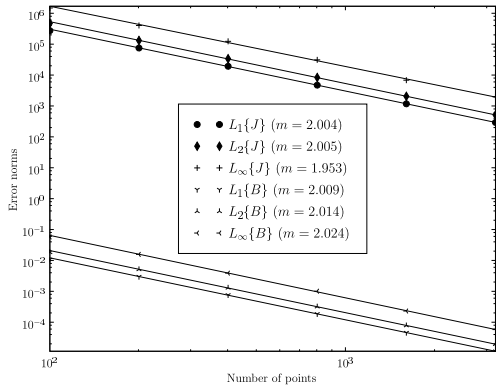


(b)

Figure 4: Convergence of **B** and **J** for isotropic Gaussian pulse problem for (a) uniform node distribution, (b) distorted node distribution. Convergence rates (labeled $m$) are given for each norm.

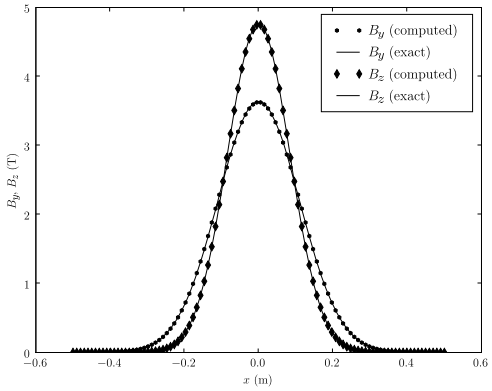


(a)

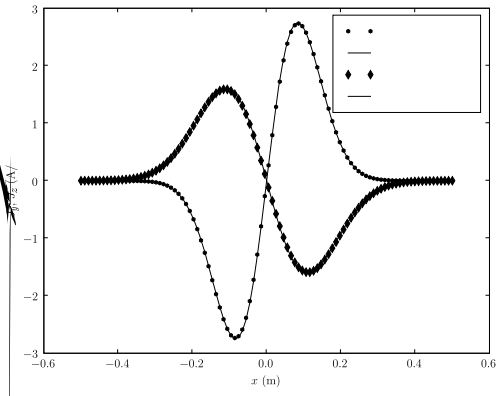


sult of its manufacture, perhaps), and that its resistivity is given by

$$\boldsymbol{\eta} = \frac{\mu_0}{100}\begin{pmatrix} 1 & 0 & 0 \\ 0 & 1 & 0 \\ 0 & 0 & 2 \end{pmatrix}$$

The way that the equations for $B_y$ and $B_z$ are coupled by Eq. 5, $\eta_{yy}$ determines the rate of decay for $B_z$, as $\eta_{zz}$ does for $B_y$. Therefore we may define directional magnetic diffusivities $D_y = \eta_{zz}/\mu_0$ and $D_z = \eta_{yy}/\mu_0$ and use the Gaussian solutions $G_{D_y}$ and $G_{D_z}$ for $B_y$ and $B_z$, respectively. In this case, $B_y$ decays roughly twice as fast

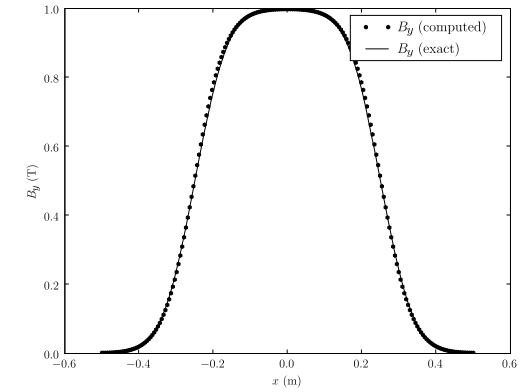


(a)

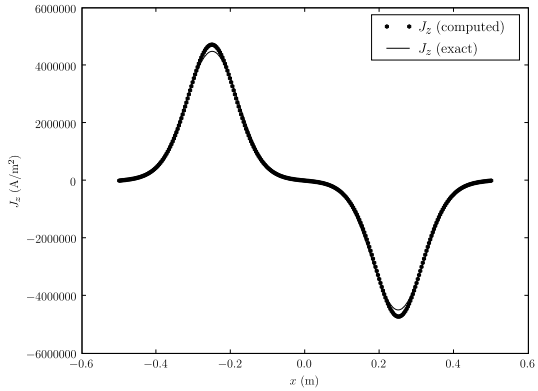


(b)

Figure 8: (a) Computed decaying square pulse solution for **B** at $t = 0.25$ s, and (b) associated current density

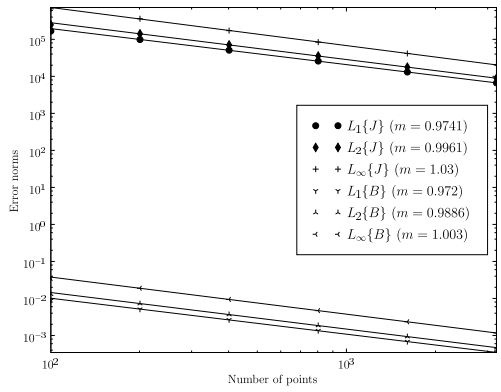


(a)

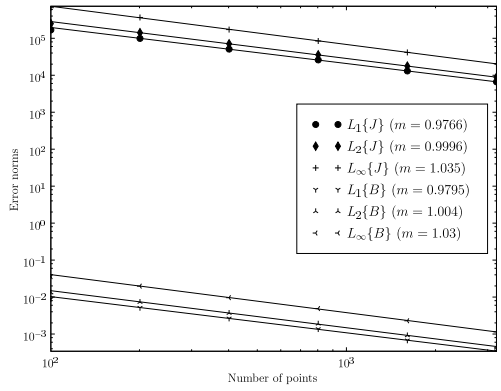


(b)

Figure 9: Convergence of **B** and **J** for decaying square pulse problem with (a) uniform node distribution, (b) distorted node distribution. Convergence rates (labeled $m$) are given for each norm.

The computed solutions at $t = 0.25$ s are shown in Fig. 8 and their convergence is shown in Fig. 9, with no significant difference between the uniform and distorted point distributions. We obtain first-order converge in all norms in both **B** and **J**, proving that this MLPG method can reliably treat problems with discontinuities.

### *6.3 Moving Pulse*

Having established that the present method successfully simulates the decay of a magnetic field within a stationary conducting medium, we now consider the same problem applied to a rigid moving conductor. Specifically, we place Gaussian and square-shaped initial magnetic fields into a conductor that is moving with velocity $v = v_0$ in the $\hat{\mathbf{x}}$ direction to ensure that the motion of the conductor does not affect the solution. With an eye toward combining the MLPG method with a Lagrangian mesh-free hydrodynamics method such as SPH, we evolve the positions of the nodes according to

$$\frac{dx}{dt} = v_0$$

with $v_0 = 1.0$ m/s and make the substitution $x \to x - v_0 t$ in the solutions of the aforementioned problems. The initial conditions and subsequently

computed solutions for a Gaussian pulse moving to the right and followed by a square pulse are shown in Fig. 10 and Fig. 11. Not surprisingly, the convergence rates for the solutions of the Gaussian and square pulses within the rigid moving are identical to those for the stationary one, since we are moving the coordinates on which the solution is defined and not the solution itself. This demonstrates the ease with which a Lagrangian representation of a problem can treat moving signals. In the Eulerian frame, where the nodal coordinates remain fixed and the solution moves, flux limiting is needed to prevent spurious oscillations and distortions [Van Leer (1974), Lin and Atluri (2001)]. Moreover, the flux limiting must often be adjust to accommodate signals of different shapes ( as Gaussian and square pulses). No suc ment is necessary here.

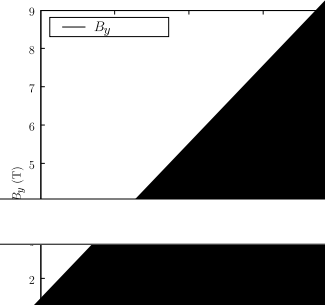

We construct an initial magnetic field $B_y(x,0)$ out of a randomly-generated polynomial that fits the boundary conditions and then compute its Fourier coefficients $\{a_n\}$. Then we evolve the system along the time interval $[0,0.2]$. The convergence rates for **B** and **J** are shown in Fig. 12. As with the other continuous problems we have demonstrated, we achieve second-order convergence in both quantities, with slightly lower rates for the distorted point distribution than for the uniform one. This could result from the fact that we have not adjusted our support radii to accommodate the disordered point positions. Nevertheless, both distributions produce convergent results, demonstrating that the technique can accurately treat homogeneous essential boundary conditions.

#### 6.4.2 *Homogeneous Natural Boundary Conditions*

The solution to Eq. 5 with $\frac{\partial B_y}{\partial x}(0,t) = \frac{\partial B_y}{\partial x}(L,t) = 0$ is the Fourier cosine series

$$B_y(x,t) = \sum_{n=0}^{\infty} b_n \cos\left(\frac{n\pi x}{L}\right) \exp\left(-\frac{Dn^2\pi^2 t}{L^2}\right)$$

with corresponding coefficients

$$b_n = \frac{2}{L}\int_0^L B_y(x,0)\cos\left(\frac{n\pi x}{L}\right) dx$$

The current density for this solution is

$$J_z(x,t) = -\frac{\pi}{\mu_0 L}\sum_{n=0}^{\infty} n b_n \sin\left(\frac{n\pi x}{L}\right) \exp\left(-\frac{Dn^2\pi^2 t}{L^2}\right) \tag{38}$$

As with the sine series, we construct an initial magnetic field $B_y(x,0)$ from a randomly-generated polynomial that fits the boundary conditions and then compute its Fourier coefficients $\{b_n\}$. Likewise, we compute the solution on the time interval $[0,0.2]$. The convergence rates for **B** and **J** are shown in Fig. 13. Again, we observe second order convergence, showing that the method works with homogeneous natural boundary conditions even when the supports of its trial and test functions overlap the domain boundary. As we have observed with previous tests, the convergence rates for the uniform and distorted point distribution are similar.

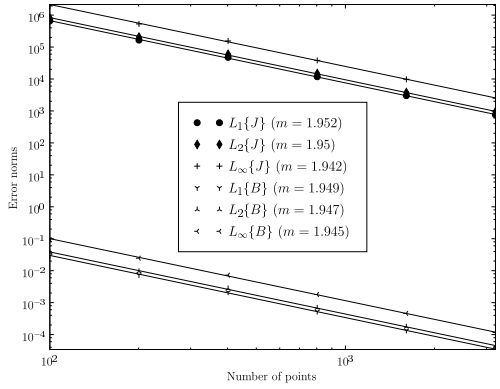


(a)

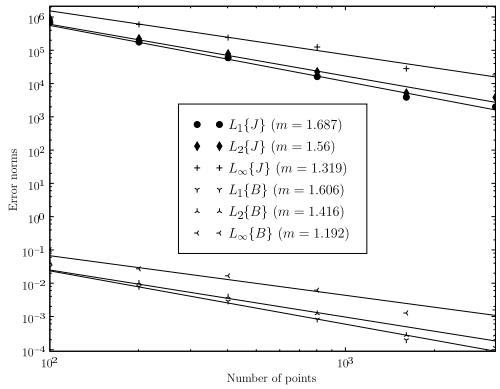


(b)

Figure 12: Convergence of **B** and **J** for Fourier sine series with (a) uniform node distribution, (b) distorted node distribution. Convergence rates (labeled $m$) are given for each norm.

### 6.5 *Oscillating Field at the Boundary*

To verify that the method can represent time-dependent essential boundary conditions, which are relevant to problems in current-driven plasma acceleration as well as those involving dynamic external magnetic fields, we consider a conductor with an oscillating external field at one of its boundaries. This problem is sometimes called the "wine cellar problem", as its application to the heat equation can be used to estimate the depth at which a wine cellar should be buried to minimize effects from fluctuations in the outside temperature. This problem has been used to verify

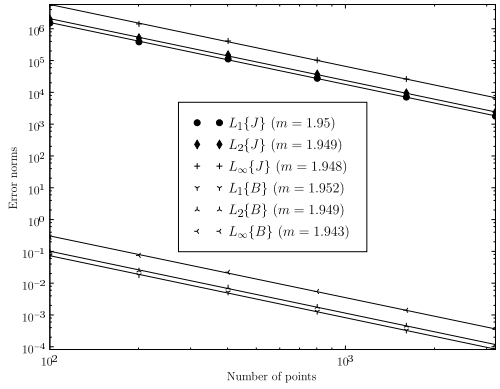


(a)

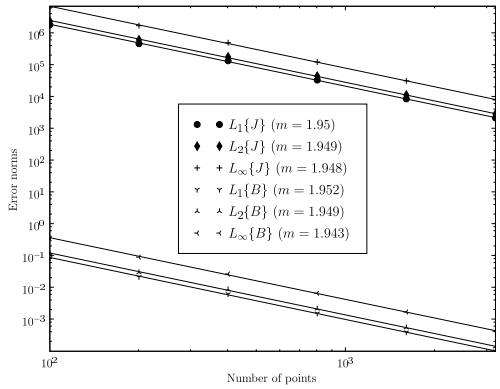


(b)

Figure 13: Convergence of **B** and **J** for Fourier cosine series with (a) uniform node distribution, (b) distorted node distribution. Convergence rates (labeled *m* are given for each norm.

the Vector Finite Element Method for magnetic diffusion problems of the sort in which we are interested [Rieben and White (2006)].

Once again, we consider a domain $[0,L]$ with an oscillating external magnetic field $B_z(0,t) = \cos(\omega t)$. The solution to Eq. 5 is the real part of the complex expression:

$$B_z(x,t) = \frac{\sin(\beta(L-x))}{\sin(\beta L)} \exp(-i\omega t)$$

with $\beta = \sqrt{\frac{i\Omega}{D}}$. The current density in this case is the real part of

$$J_y(x,t) = \frac{1}{\mu_0}\beta \frac{\cos(\beta(L-x))}{\sin(\beta L)} \exp(-i\omega t)$$

We choose $D_m = 0.01$ and $L = 1$ and evolve the system to $t = 0.5$ s. The computed solutions for **B** and **J** are shown in Fig. 14. The error for both quantities converges at second order, as shown in Fig. 15. This means that problems with non-homogeneous and time-dependent essential boundary conditions can be accurately treated with this method. Note that the essential boundary conditions must be enforced at $t^{n+1}$ (and not $t^n$) in order to achieve second-order convergence. Again, the uniform and distorted point distributions yield no significant difference in the convergence of the error norms.

### 6.6 Manufactured Nonlinear Solutions

The Method of Manufactured Solutions (MMS) provides a way to generate analytic solutions with complex structure for the verification of a numerical method [Roache (2002)]. Since analytic solutions to nonlinear differential equations are scarce, we use the MMS to generate a solution to Eq. 5 that demonstrates the ability of the technique to model magnetic fields in conductors with more complicated electrical resistivities than we have used so far.

To test a manufactured solution that yields a time-dependent resistivity, we begin with the solution (and corresponding current density)

$$\begin{aligned} B_y(x,t) &= \frac{\cos x}{t} \\ J_z(x,t) &= -\frac{\sin x}{\mu_0 t} \end{aligned} \tag{39}$$

on the domain $[0,1]$. Substituting Eq. 39 into Eq. 5, we find that the corresponding resistivity is $\eta(x,t) = \mu_0/t$. We also use Eq. 39 to specify essential boundary conditions. We then run a simulation along the time interval $[1,1.1]$, with a fixed step size determined by the characteristic time scale in Eq. 7 with $\eta = \eta(x,1)$, but scaled linearly with the nodal spacing instead of quadratically.

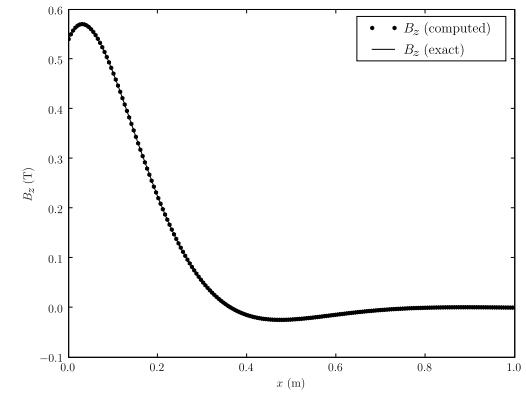


(a)

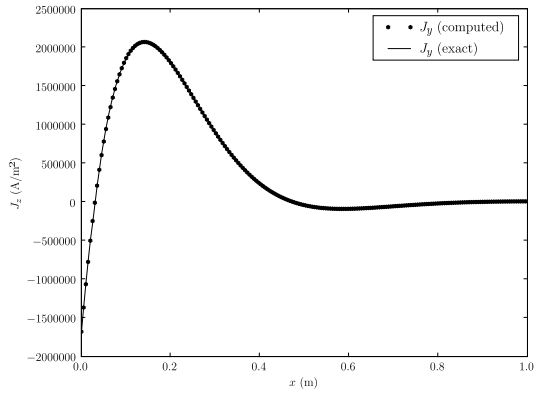


(b)

Figure 14: Computed (a) magnetic induction and (b) current density for wine cellar problem at $t = 0.5$ s

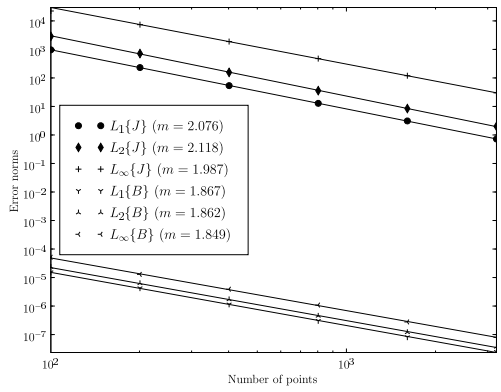


(a)

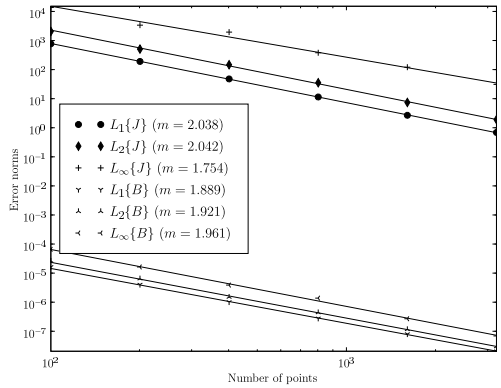


(b)

Figure 15: Convergence of **B** and **J** for wine cellar problem with (a) uniform node distribution, (b) distorted node distribution. Convergence rates (labeled $m$) are given for each norm.

The convergence rates for **B** and **J** are shown in Fig. 16, and are second-order as expected. This means that our treatment of time-dependent resistivities, as specified by Eq. 31, is sufficient to achieve the expected convergence rate with little difference in the uniform and distorted point distributions.

Our second manufactured solution tests a spatially inhomogeneous and time-dependent resistivity, where the non-zero components of **B** and **J** are

$$\begin{aligned} B_y(x,t) &= 1+x+t \\ J_z(x,t) &= \frac{1}{\mu_0} \end{aligned} \tag{40}$$

Here, the resistivity is given by $\eta = \mu_0(1+x+t)$, and the essential boundary conditions are prescribed according to Eq. 40. Again, we compute the solution on the domain $[0,1]$ for the time interval $[1,1.1]$, fixing the step size this time according to $\eta = \eta(x,1.1)$, its maximum value. The second order MLS shape functions can exactly represent the solution, which is linear in space and time, and so we obtain a solution for **B** at machine precision ( $10^{-14}$) and for **J** at 6 orders of magnitude greater ($10^{-14} \times \mu_0^{-1} \approx 10^{-8}$). Thus, the method can treat spatially-inhomogeneous and time-dependent resistivities at machine precision with both the uniform and distorted point distributions.

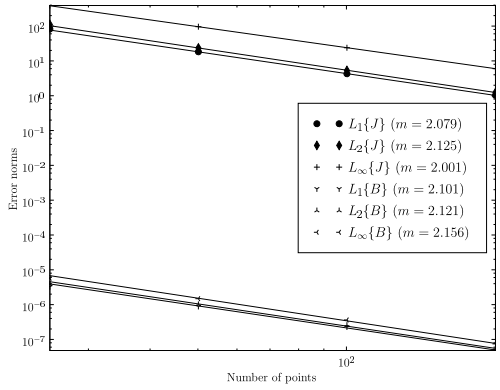


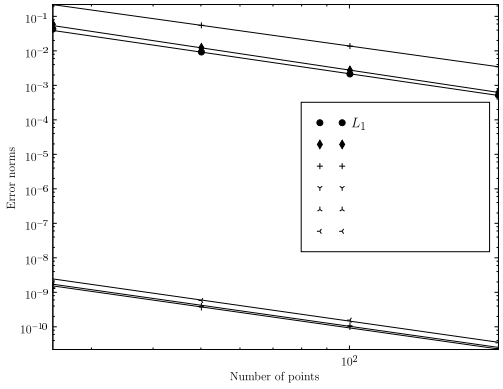


(a)

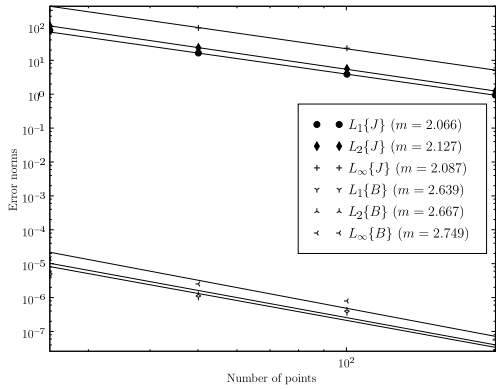


(b)

Figure 16: Convergence of **B** and **J** for $B_y(x,t) = \cos x/t$ with (a) uniform node distribution, (b) distorted node distribution. Convergence rates (labeled $m$) are given for each norm.

Our third manufactured solution is defined with the following non-zero components of **B** and **J**:

$$\begin{aligned} B_y(x,t) &= \sqrt{1+2\mu_0 x+2\mu_0 t} \\ J_y(x,t) &= \frac{1}{\sqrt{2\mu_0 x+2\mu_0 t}} \end{aligned} \tag{41}$$

which yields $\eta = \mu_0(1+2x+2t)$. Computing the solution once again on the domain $[0,1]$ on the time interval $[1,1.1]$, we obtain similarly convergent results, as shown in Fig. 17.

typically around $10^{-5}$.

The one-dimensional test problems presented demonstrate the successful treatment of relevant boundary conditions, anisotropic diffusion, rigidly moving conductors, discontinuous magnetic fields, inhomogeneous and time-dependent models for electrical resistivity. Thus we can expect this method to give good results in realistic magnetic diffusion problems.

Much work remains in the study of this method. We are interested in exploring a MLPG5 formulation (in which the test functions are the Heaviside step function) to alleviate some of the complexity we faced in computing the integrals in Eq. 16. Another benefit of this variant is that it allows the use of smaller test and trial function support domains, improving the conditioning of the linear system and lessening the computational effort for large problems. Many practitioners of MLPG methods have put MLPG5 to good use in elastodynamics [Atluri, Han, and Rajendran (2004)] and other challenging problems.

Our primary motivation for exploring this method, though, is the development of a mesh-free method for studying magnetohydrodynamics (MHD), which describes the dynamics of magnetic fields within deformable moving conductors. Other mesh-free methods such as Gradient Particle Magnetohydrodynamics (GPMHD) [Maron and Howes (2003)] and Smoothed Particle Magnetohydrodynamics (SPMHD) [Price and Monaghan (2004)] have shown great promise in treating ideal MHD, which deals exclusively with fields in perfect conductors. Now that we have established its worth in treating the diffusion associated with imperfect conductors, we hope to combine this MLPG method with one of these methods to extend their capabilities. This will be the main emphasis of future work.

In treating more realistic and physically relevant problems, we will also extend the technique to solve fully three-dimensional problems, and to adapt the radii of the trial functions dynamically to disordered distributions of points. Our analysis so far has been general enough to describe a three-dimensional spatial discretization; it remains for us to produce a functional 3D implementation.

**Acknowledgement:** The authors wish to thank Dr. Zhidong Han for his helpful suggestions regarding the details of implementing MLPG methods. J. Johnson is supported by a Lawrence Livermore National Laboratory Student Employee Graduate Research Fellowship (SEGRF).

This work was performed under the auspices of the Department of Energy by the University of California, Lawrence Livermore National Laboratory under contract No. W-7405-Eng-48.

## References

**Atluri, S. N.** (2004): *The Meshless Method (MLPG) for Domain and BIE Discretizations*. Tech Science Press, Forsyth, GA.

**Atluri, S. N.; Han, Z. D.; Rajendran, A. M.** (2004): A New Implementation of the Meshless Finite Volume Method, Through the MLPG "Mixed" Approach. *CMES: Computer Modeling in Engineering and Sciences*, vol. 6, pp. 491–513.

**Atluri, S. N.; Kim, H. G.; Cho, J. Y.** (1999): A critical assessment of the truly Meshless Local Petrov-Galerkin (MLPG) and Local Boundary Integral Equation (LBIE) methods. *Comput. Mech.*, vol. 24, pp. 348–372.

**Atluri, S. N.; Liu, H. T.; Han, Z. D.** (2006): Meshless local Petrov-Galerkin (MLPG) mixed collocation method for elasticity problems. *CMES: Computer Modeling in Engineering and Sciences*, vol. 14, pp. 141–152.

**Atluri, S. N.; Liu, H. T.; Han, Z. D.** (2006): Meshless Local Petrov-Galerkin (MLPG) Mixed Finite Difference Method for Solid Mechanics. *CMES: Computer Modeling in Engineering and Sciences*, vol. 15, pp. 1–16.

**Atluri, S. N.; Zhu, T.** (1998): A new meshless local Petrov-Galerkin (MLPG) approach in computational mechanics". *Comput. Mech.*, vol. 22, pp. 117–127.

**Balay, S.; Buschelman, K.; Gropp, W. D.; Kaushik, D.; Knepley, M. G.; McInnes, L. C.; Smith, B. F.; Zhang, H.** (2001): PETSc Web page, 2001. http://www.mcs.anl.gov/petsc.

**Belytschko, T.; Krogauz, Y.; Organ, D.; Fleming, M.; Krysl, P.** (1996): Meshless methods: an overview and recent developments. *Comp. Meth. Appl. Mech. Engn.*, vol. 139, pp. 3–47.

**Bottauscio, O.; Chiampi, M.; Manzin, A.** (2006): Element-free galerkin method in eddy-current problems with ferromagnetic media. *IEEE Transactions on Magnetics*, vol. 42, pp. 1577–1584.

**Brauer, J. R.; Mayergoyz, I. D.** (2004): Finite-element computation of nonlinear magnetic diffusion and its effects when coupled to electrical, mechanical, and hydraulic systems. *IEEE Transactions on Magnetics*, vol. 40, pp. 537–540.

**Chen, F. F.** (1984): *Introduction to Plasma Physics and Controlled Fusion*. Plenum Publishing, New York, NY.

**Chinchapatnam, P. P.; Djidjeli, K.; Nair, P.** (2006): Unsymmetric and symmetric meshless schemes for the unsteady convection-diffusion equation. *CMAME*, vol. 195, pp. 2432–2453.

**Davidson, P. A.** (2001): *An Introduction to Magnetohydrodynamics*. Cambridge University Press.

**Diltz, G. A.** (1999): Moving-Least-Squares-Particle Hydrodynamics - I. Consistency and Stability. *International Journal for Numerical Methods in Engineering*, vol. 44, pp. 1115–1155.

**Gruneisen, E.** (1933): *Ann. Physik*, vol. 16, pp. 530.

**Hwang, D. Q.; Horton, R. D.; Howard, S.; Evans, R. W.; Brockington, S. E.** (2006): Advances in CTIX Accelerator Study. *Journal of Fusion Energy*, vol. 1, no. 1-2, pp. 81–84.

**Hyman, J.; Shashkov, M.** (2001): Mimetic finite difference methods for maxwell's equations and the equations of magnetic diffusion, 2001.

**Jackson, J. D.** (1999): *Classical Electrodynamics*. John Wiley and Sons, Inc., New York, NY.

**Lin, H.; Atluri, S. N.** (2000): Meshless Local Petrov-Galerkin (MLPG) Method for Convection-Diffusion Problems. *CMES: Computer Modeling in Engineering and Sciences*, vol. 1, pp. 45–60.

**Lin, H.; Atluri, S. N.** (2001): The Meshless Local Petrov-Galerkin (MLPG) Method for Solving Incompressible Navier-Stokes Equations. *CMES: Computer Modeling in Engineering and Sciences*, vol. 2, pp. 117–142.

**Maron, J. L.; Howes, G. G.** (2003): Gradient Particle Magnetohydrodynamics: A Lagrangian particle code for astrophysical magnetohydrodynamics. *ApJ*, vol. 595, pp. 564–572.

**Monaghan, J. J.** (1992): *Mon. Not. R. Astron. Soc.*, vol. 30, pp. 543.

**Nayroles, B.; Touzot, G.; Villon, P.** (1992): Generalizing the Finite Element Method: Diffuse Approximation and Diffuse Elements. *Comput. Mech.*, vol. 10, pp. 307–318.

**Price, D. J.; Monaghan, J. J.** (2004): Smoothed Particle Magnetohydrodynamics - I. Algorithm and tests in one dimension. *Mon. Not. R. Astron. Soc.*, vol. 348, pp. 128–138.

**Rieben, R.; White, D.** (2006): Verification of high-order mixed finite element solution of transient magnetic diffusion problems. *IEEE Trans. Magnetics*, vol. 42, pp. 25–39.

**Roache, P. J.** (2002): Code Verification by the Method of Manufactured Solutions. *ASME Journal of Fluids Engineering*, vol. 124, no. 1, pp. 4–10.

**Sterk, M.; Robic, B.; Trobec, R.** (2005): Meshfree Method Applied to the Diffusion Equation. In Vajtersic, M.; Trobec, R.; P., Z.; Uhl, A.(Eds): *Parallel Numerics '05*, volume 1.

**Stoer, J.; Bulirsch, R.** (1991): *Introduction to Numerical Analysis*. Springer, New York, NY.

**Van Leer, B.** (1974): Towards the ultimate conservative difference scheme II. Monotonicity and conservation combined in a second order scheme. *J. Comp. Phys.*, vol. 14, pp. 361–370.

**Zhu, T.; Atluri, S. N.** (1998): A modified collocation method and a penalty formulation for enforcing the essential boundary conditions in the element free Galerkin method. *Comput. Mech.*, vol. 21, pp. 211–222.

**Zienkiewicz, O. C.; Taylor, R. L.** (1989): *The Finite Element Method, Volume 1: Basic Formulations and Linear Problems*. McGraw-Hill.